Available online at www.sciencedirect.com
ScienceDirect
Journal of Bionic Engineering 4 (2007) 063–076

Biomimetics of Campaniform Sensilla: Measuring Strain from the Deformation of Holes

Julian F. V. Vincent[1], Sally E. Clift[1], Carlo Menon[2]

1. *Department of Mechanical Engineering, The University of Bath, Bath BA2 7AY, UK*
2. *Advanced Concepts Team, European Space Agency, 2201 AZ Noordwijk, The Netherlands*

Abstract

We present a bio-inspired strategy for designing embedded strain sensors in space structures. In insects, the campaniform sensillum is a hole extending through the cuticle arranged such that its shape changes in response to loads. The shape change is rotated through 90° by the suspension of a bell-shaped cap whose deflection is detected by a cell beneath the cuticle. It can be sensitive to displacements of the order of 1 nm. The essential morphology, a hole formed in a plate of fibrous composite material, was modelled by Skordos *et al.* who showed that global deformation of the plate (which can be flat, curved or a tube) induces higher local deformation of the hole due to its locally higher compliance. Further developments reported here show that this approach can be applied to groups of holes relative to their orientation.

The morphology of the sensillum in insects suggests that greater sensitivity can be achieved by arranging several holes in a regular pattern; that if the hole is oval it can be "aimed" to sense specific strain directions; and that either by controlling the shape of the hole or its relationship with other holes it can have a tuned response to dynamic strains.

We investigate space applications in which novel bio-inspired strain sensors could successfully be used.

Keywords: campaniform sensillum, strain, displacement, compliance, hole, remote sensing, fibrous composite

1 Introduction

Maintaining the integrity and intactness of a mechanical structure is important to ensure safety and to prevent accidents caused by vibration and structural fatigue. In such systems, the measurement of strain as one of the parameters is necessary. We therefore need high quality strain sensors, whether independent or integrated into an intelligent material. Strain measurement can also be proved for proprioceptive feedback in robots, tools, and other structures, giving the ability to monitor their own movements and loads and respond to them.

During a collaboration between the University of Bath and the Advanced Concepts Team of the European Space Agency, we reviewed state-of-the-art of strain measurement systems for space applications and proposed a biomimetic technique to mechanically amplify local displacements of space structures.

Embedded strain sensors are of interest for many space applications, especially when slender systems (solar panels, booms, solar sails, *etc.*) or structural frames must be monitored during hazardous mission phases. Strain sensors can also be used as force sensors, especially when they are embedded in cantilevers. They could be used in several systems including unlocking systems, docking mechanisms, limit switch devices, robotic arms.

The application and the environment strongly determine the performance required of the sensor. A main distinction concerns sensors for ground or space use.

Strain sensors are widely used in *ground tests* of space hardware. In this case, sensors are added to the payloads and structures. Integration of this kind of sensor in the hardware is generally not required. During

Corresponding author: Julian F. V. Vincent
E-mail: j.f.v.vincent@bath.ac.uk

ground testing, strains are of interest to confirm numerical simulations and to verify if the hardware satisfies the required specifications. Thermal deformation, in particular, can induce non-negligible stresses, leading to thermo-elastic failures of the structure. Thermal deformation can also determine poor performance of the payload (especially in the case of optical payloads), and bearings and mechanisms to seize and malfunction.

Deformation measurements *in space*, on the other hand, require the sensors to be embedded in the space structure, and power to be supplied by the space system itself. Strain sensors must also withstand the harsh space environment and cope with radiation, vacuum, a wide thermal range, vibration, and other space disturbances. The sensor should also comply with the accuracy and linearity requirements of the particular application, and be of adequate size (nano, micro, mini, or macro scale). Strain deformations are measured in several circumstances in space scenarios, including when it is necessary to monitor spacecraft health, feed-back signals in active control systems, or perform scientific investigations. Monitoring space system deformations is of interest especially when counter-measure can be taken. For instance, in the active control of a slender structure used to damp mechanical vibrations, strain monitoring assumes fundamental importance. Also in force-feedback of a robotic manipulator or in automatic docking, the force measurement at the interface, often sensed through strain measurements, is fundamental to the success of the operations.

Promising technologies that will probably find application in future missions will greatly benefit from extensive use of strain sensors distributed and integrated in the space vehicle structure. For instance, gossamer structures, inflatable locomotion systems, solar sails, and other compliant structures and mechanisms, may be controlled via the use of a sensor network distributed on their surfaces and lattices.

1.1 Current strain measurement systems

A wide variety of methods can be used to sense deformation in space structures. No method is exclusive and new circumstances and applications may require the use of novel strain sensors.

One of the most popular sensors is the strain gauge. This deformation sensor is usually made of a conducting foil supported by an insulating backing which is attached to the structure through a suitable adhesive. The deformation imposed on the foil by the structure makes the electrical resistance change. A Wheatstone bridge is commonly used to monitor the variation of electrical resistance. Piezoresistive silicon thin film has a higher gauge factor than the common metal foil strain gauges and its integration within MEMS structures has made it possible to measure strain within a composite structure without extensive wiring. The monofilament piezoresistive strain sensor, however, still performs inconsistently with different gauge factors when the sensor is loaded in or out of plane. This problem can be partially solved by making piezoresistive membrane strain sensors, which has a similar gauge factor during bending and axial loading, and with comparable gauge factor sensitivity[1].

Strain gauges are often used during spacecraft ground testing, as a large number of strain gauges can be attached to surfaces and then removed without damaging the structure. Strain gauges are however external bodies, and therefore their presence may disturb the deformation pattern, especially on ultra-thin structures. In addition, they cannot withstand large deformations, and their accuracy strongly depends on the attaching interface. Thermal deformation can also compromise the accuracy of the measurement.

Another typical method of measuring local deformation is based on the piezoelectric effect. Quartz, synthetic crystals, polarized ferroelectric ceramics, and some polymers, display reversible electro-mechanical energy conversion when deformed. The piezoelectric sensor can be designed to respond to several kinds of mechanical deformation, such as thickness shear, face shear, thickness expansion, and transverse expansion. These materials have been widely considered for space applications. The possibility of using them also as actuators was considered and implemented for active control of structures. The development of micromachining technologies now allows the fabrication of miniaturized piezoelectric sensors that can also be embedded in structures.

Electro-optical measurement systems, which combine optical and electronic principles, represent another category of deformation sensors which is of interest for space engineering. In 1967, Menadier *et al.*[2] proposed the "Photonic Sensor" that used fibre optics to measure displacements. Interferometric systems, such as the Michelson interferometer or other advanced techniques, allow very accurate measurements. When the structure is made of composite materials, electro-optical systems can easily be embedded, thus allowing continuous monitoring. However, their integration in the structure is often difficult to implement, and the mechanical resistance that this system exhibits can compromise the quality of the measurements.

Imaging techniques represent another way of detecting deformations. These techniques rely on the acquisition of images by one or more cameras and on the data processing needed for the reconstruction of displacements with time. Imaging measuring systems have the advantage of being non-contact and so do not introduce disturbances into the measurement of the deformation. However, they need to have a precisely positioned camera with respect to the surface to be monitored, thus complicating their utilization, especially on orbit.

Another method is based on the birefringence that some transparent materials show under strain. Reflective photo-elasticity presents some advantages as the material can be used as a coating, although the thickness must be finely controlled.

Translation can be also monitored by taking advantage of variation in capacitance of a capacitor. Miniaturization using MEMS technology is possible and increases the opportunity of using such a displacement system. The integration of this kind of system into space structures is often challenging although good performance can be obtained.

Several studies have been carried out to obtain reliable strain sensors specifically for space applications. Wnuk *et al.*[3] investigated a weldable strain gauge employing the NASA Lewis PdCr/Pt wire strain sensor; Ounaies *et al.*[4] focused on the development of high temperature piezoelectric polymers for active flow control sensors and health monitoring sensors; Mckenzie *et al.*[5] investigated the use of fibre optic sensing in space structures to provide critical information about the spacecraft health during fabrication, testing and service lifetime; Udd *et al.*[6] analyzed and tested transversely loaded fibre grating strain sensors for aerospace applications; and many other researchers in industry and universities have worked on this area, achieving remarkable results.

New technologies are emerging. Wireless systems, capable of transmitting deformation signals without the need to increase the spacecraft harness, have been miniaturized (e.g. the MicroStrain® wireless strain gauge) and are easy to integrate and use. *Ad hoc* wireless sensor networks are under development for use in space systems and preliminary results are promising[7]. Another technology that could lead to outstanding performance in far future space applications relies on the mechanical deformation of nanotubes which induces noticeable changes in their conductance, as their electronic properties are a strong function of their atomic structure[8].

All these strain sensors rely on measuring deformations of a structure, without taking advantage of possible mechanical amplifications of the signal due to a modification of the structure itself. Natural systems, on the other hand, locally amplify deformations by arrays of micro holes. The strategy proposed in this paper is to take advantage, as nature does, of micro-holes present in engineering systems to increase precision of local deformation measurements. The shape and geometry of individual miniaturized holes could also be determined and selected to sense deformation in particular directions. By combining arrays of differently shaped holes, optimal strain mapping is theoretically possible. This strategy can, in principle, take advantage of most of the aforementioned strain measurement systems in order to transduce the amplified mechanical deformation into an electrical signal.

The proposed strategy could allow easy integration of the measuring system in composite structures in which miniaturized cavities could be formed during fabrication. Tri-axial composites[9], which are of particular interest for the manufacture of several space structures (including large antennas[10]), have a

particularly suitable configuration for the proposed sensors.

Holes have been used in a stress-concentrating region to improve sensitivity in piezoresistive silicon cantilevers for scanning probe microscopy[11]. But a blind hole to concentrate strain, which is transduced into a signal in a microstructure and used as a stand-alone strain sensor, has been reported only by Wicaksono[12]. Engineering mechanics teaches that holes are commonly stress concentrators and crack initiators, not sources of information for sensor engineers. The membrane in a blind hole serves to amplify the strain in the wafer. However the sensitivity of strain sensors could be further enhanced by learning from strain sensors found in biology, for instance the campaniform sensillum of insects. Its unique structure yields strain amplification that enables more sensitive strain detection, even when associated with a stiff material.

The design of space structures is driven by stringent stiffness requirements as their modal nodes should not couple with launcher vibrations. We here want to highlight that the introduction of micro-holes increases local strains but decreases natural vibrations negligibly. Therefore the strategy here proposed has high potential for use in space systems. As an example, Fig. 1 shows an aluminium plate having length of 0.1 m, width of 0.1 m, and thickness of 5 mm. The plate was modelled as a shell using Finite Element Method, almost 100 000 elements were used. Both rotations and translations of the four edges of the plate were constrained. The first natural frequency of the plate with and without a micro hole (diameter of 100 μm) was computed. The variation of

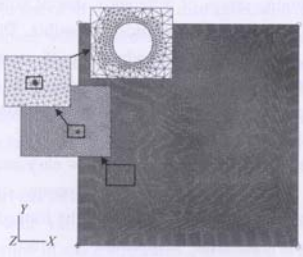

Fig. 1 Plate with micro-hole. The zoom shows the geometry of the mesh.

such frequency, as foreseen, was negligible (2×10E−6%) and this implies that the stiffness of the plate does not change when a micro-hole is introduced.

1.2 The campaniform sensillum

The campaniform sensillum is essentially a hole in a plate with a bell-shaped (hence "campaniform") cap suspended in its centre (Fig. 2). Campaniform sensilla are found in animals that have an external skeleton (arthropods) that can be characterised[13] as a composite material of chitin nanofibres (Young's modulus in excess of 150 GPa) in a protein matrix (Young's modulus ranging from 1 kPa to 15 GPa) with various fillers (e.g. calcium carbonate in aquatic crustacea).

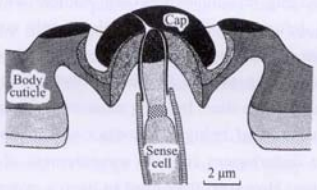

Fig. 2 Section through a campaniform sensillum.

They were recognised as strain sensors by Pringle who studied sensilla on the legs of the cockroach[14]. They are arranged in groups at the joints, being oval with parallel orientation of the sensilla of a group. The sensilla vary in shape and size, but are rarely circular and sometimes long and narrow. Their length varies from 6 to 24 μm. They are arranged more or less regularly in lines, with the long diameters of the sensilla diagonal to the direction of the lines. Sometimes there is indication of a second alignment, at an angle to the first. When this is apparent, the direction of the long diameters of the sensilla bisects the angle between the two lines. In section there are several different morphologies; Pringle figured six from various insects and various authors.

The geometry and mechanical properties of the suspension cause the cap to move up and down as the hole changes its dimensions when the plate is stretched, compressed, bent or twisted. Thus the cap system rotates deformation in the plane of the plate through 90°, allowing the deformation to be detected out of the plane[14,15]. In insects the sensillum, together with its

associated sensory and nerve cells, forms a simple yet sensitive mechanism[16,17] which is capable of detecting displacements of the order of a nanometer[18]. The plate in which the sensillum is formed can be anisotropic depending on the orientation of the chitin fibres and heterogeneous depending on the volume fractions of the components, degree of cross-linking of the matrix, *etc.* There is therefore considerable freedom in the design parameters. In most arthropods (including insects and crustaceans) the sensillum hole is oval, so it can be "aimed" and pick up and amplify displacements in defined directions[14,19,20].

A classification of campaniform sensilla using morphological criteria has been developed[21]. All variations of the two most important outer structural elements, the "cuticular cap" and the "cuticular collar", were taken into consideration: (a) the external shape of the cuticular cap; (b) the position of the cuticular cap in relation to the remaining cuticle; (c) the position of the cuticular collar in relation to the cuticular cap. This resulted in a classification of campaniform sensilla into 24 types. This typology was applied to the campaniform sensilla of *Calliphora*, which show considerable variations in their outer structures. Using scanning and transmission electron microscopy only 9 out of the 24 different types of campaniform sensilla were found in the fly. In addition to the morphology, a limited amount of information can be gleaned about the mechanical properties of the components by considering their reaction with various histological stains. Put simply, a mixture of stains such as "Mallory's Trichrome" can pick out hydrophilic, lipophilic, *etc.*, tissues, which suggests the amount of water or (hydrophobic) cross-linking agent they might contain, and hence the mechanical properties. Stiff cuticles tend to have a modulus of about 1 GPa or more, more rubbery cuticles, probably containing significant amounts of resilin, a rubber-like cuticle, have a modulus of 1 MPa, and a few cuticles are even softer[13]. The cuticular cap and the upper region of the collar consist of tanned, non-lamellated cuticle which does not stain with Mallory's triple stain. This suggests that it is almost entirely unreactive and that all the cross-linking sites are occupied, rendering the cuticle stiff and dry. Modulus may be as high as 15 GPa. It shows no UV-fluorescence, (UV-fluorescence is one of the diagnostic characteristics of resilin). On the other hand the caps of campaniform sensilla on the cockroach leg show resilin-like viscoelasticity[22] which cannot be explained by the properties of solid cuticle. Therefore the spongy cuticle which suspends the cap in the middle of the hole, which appears transparent in the TEM, probably consists of resilin.

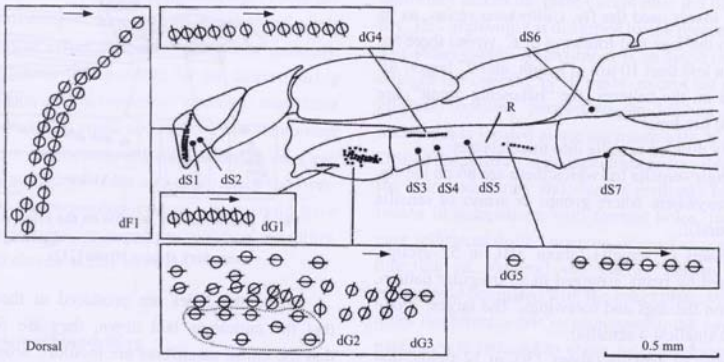

Fig. 3 Sensilla along the wing of a fly (from [21]).

Most sensilla are oval; when they occur in groups, which is usual, the long axis of each sensillum in the group is orientated in much the same direction[23]. For instance on the wing of a fly there is a group arranged along the base of one of the main structural beams ("veins"), orientated at 60° to its long axis, which therefore can detect torsion (Fig. 3, group dG4 and part of group dG3). In the same insect the sensilla in the base of the halteres (planar gyroscopes) occur in trapezoidal arrays[24] (Fig. 4). Holes with greater width: length ratios are subject to greater deformations. The greatest deformation occurs when a plate containing an elliptical hole is loaded orthogonal to the major axis of the hole. This essentially alters the stress-strain characteristic of the plate.

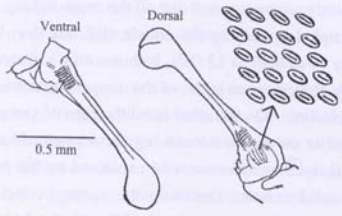

Fig. 4 Two views of a fly's haltere showing a field of campaniform sensilla.

The most complete mapping of campaniform sensilla on an insect used the fly, *Calliphora vicina*, as its subject. On the legs and forewing of *C. vicina* there are 137 sensilla less than 10 μm in length, and 27 larger. All the sensilla on the halteres (the "balancing organ") are less than 10 μm long[23].

Gnatzy divided sensilla into three classes:

- *single* sensilla (of which there are 86 on the fly, occurring anywhere where groups or arrays of sensilla are also found);
- *groups* of sensilla (about 350, in 52 groups, distinguished by being arranged in an irregular pattern, occurring on the legs and forewings. The largest group has 32, the smallest 3 sensilla);
- *fields* of sensilla (about 730, in 12 fields, distinguished by their regular pattern (Fig. 4), occurring on the halteres except for one on the tegula of the wing. About 670 campaniform sensilla, more than 55% of all sensilla, are localized in 10 fields on the halteres.).

The grouping may be a mechanism to ameliorate the crack-starting problem, since an assemblage of small holes will increase the compliance to a similar extent as a single large hole, but each hole individually is not large enough to be a threat to mechanical integrity and may even make the structure more resistant to failure, since a plate with a lattice hole structure can, under certain circumstances, endure greater loading than a plain plate[25]. However, there are other ways in which the insect apparently avoids the stress concentrating properties of an oval hole. The problem will be most severe when the hole is stretched orthogonally to its major axis. This is probably possible only when the cuticle can be loaded in a single direction. If the sensillum is on a strut which can be bent, then it is likely that the strut can be bent in more than one direction. However, in at least one case (Fig. 5) it looks as if the sensilla are making use of a Poisson ratio effect. On the main vein of the fly's wing the sensilla are arranged with the longitudinal axis parallel to the main axis of the vein (group vG3). This suggests that the vein deforms across its section on bending, tending to flatten and induce (secondary) hoop stresses. These will be less than primary the bending stresses, so the sensilla will be able to register deformation without compromising the integrity of the vein, albeit with some loss of sensitivity.

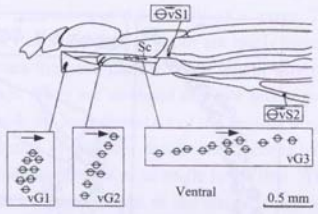

Fig. 5 Orientation of sensilla on the veins at the base of the wing of *Calliphora*, suggesting sensing of secondary strains (from [21]).

Since the holes are produced at the same time that the cuticle is laid down, they are formed such that the chitin nanofibres are moulded around the hole rather than being interrupted by it, as would happen in a crude technical system. This both reduces the stress-concentrating effect of introducing a hole in a loaded area of the skeleton by up to 50%[26], and can locally

amplify the global strain by up to an order of magnitude, thus increasing the sensitivity[15]. There is therefore the possibility that the presence of holes does not compromise unduly the global load-bearing characteristics of the structure in which they occur, but can greatly increase the strain sensitivity by controlling local compliance, a concept which is explored later in this paper. The properties of the sensillum hole can be tuned by varying the stiffness of the material surrounding it, which is present as a discrete ring[15,23].

It seems likely that the mechanics of the cap and the stiffness of its suspension will affect the dynamic response of the sensillum as a whole, although this has not been investigated.

The conceptual simplicity and operational versatility of the campaniform sensillum and related organs therefore render it a strong candidate for biomimetic study and implementation. There are associated engineering advantages in that a hole is an integral part of the structure in which it occurs and so will interact with that structure in a reliable fashion, which may not be possible with a conventional foil strain gauge which is glued on to the surface and which may therefore come unstuck. A foil strain gauge also has a temperature coefficient which has to be accounted for in the measurements, and may not be able to withstand temperatures as high (or low) as those borne by the structure it is monitoring. A hole has no such disadvantages. Since the displacement of a hole is a geometrical effect, it can be monitored remotely. Therefore not only is it possible for the strain sensing unit (the hole) to endure conditions which the transducer (a laser, or whatever) could not support, but the number of transducers can be reduced since a single laser can scan a large number of holes and thus reduce the overhead cost of the measuring system. This could have positive implications for simplicity and thus reliability. There would also be saving in weight.

2 Results

2.1 Finite element modelling

The first study on the campaniform sensillum to use finite elements was a 3-dimensional model by Chan based on the morphology described by Gruenert and Gnatzy[21]. Chan's work was combined with that of Skordos which examined the behaviour of a 2-dimensional plate with a hole in it. Both these studies were published in a single paper which is extensively quoted here since it forms the foundation of the present work.

Their main objective was to study the strain and displacement fields associated with circular or elliptical openings in laminated plates in order to investigate their potential for integrated strain sensors. Since Skordos *et al.* were therefore primarily interested in the detection of displacement, the detailed stress concentration levels associated with these openings was not of primary concern. However, strain energy density levels associated with different hole and fibre configurations were used to assess the relative likely strength reduction effect of the openings. To compare the relative strain amplification effect of drilled and formed holes of the same size in loaded plates, they used the relative change in length of diameters (circular) or semi-axes (elliptical) in directions parallel and normal to the load. A similar approach has been used in this paper.

Nearly all studies on the effect of holes in stressed components focus on the stress-concentrating effect of the hole and the increased likelihood of failure which results. In a uniform plate the strain energy is distributed uniformly across the plate except near the fixed boundary. This uniformity is disturbed by the presence of holes. The strain energy is maximum at an angle of 90° at the edge of the opening in all cases, except for the formed elliptical opening parallel to the loading where the maximum is located along the major axis of the ellipse. Drilled holes result in greater strain energy densities near the hole boundaries and steeper gradients of its distribution in comparison with formed holes. In the worst case (elliptical drilled opening orientated normal to the direction of loading) the energy density increases twenty-fold compared with the intact plate. With formed holes the effect is not so pronounced; the strain energy maximum is reduced to about half that found with the drilled hole. This is illustrated by the way the strain energy concentration relaxes from its maximum close to the hole to a low value remote from the hole. The strain

energy density is also distributed much more broadly across the specimen when the hole is formed rather than drilled. Formed holes are typically half as severe as the drilled ones.

The deformation under load of each of the elliptical holes in a regular 4 by 5 array (Fig. 6) with a common orientation was predicted using the ABAQUS finite element package. Each hole had a ratio of minor to major axis of 6.5. The array models the arrangement of campaniform sensilla at the base of a fly's haltere (Fig. 3)[27].

A single hole arrangement was also analysed for validation against the results of Skordos *et al.*[15].

Both models were meshed using 8-noded biquadratic plane stress elements (ABAQUS element type CPS8R). Following mesh sensitivity investigation, the mesh selected for the single hole model had a total of 9458 elements, and that for the multiple hole model had 12 823 elements (Fig. 7). A Young's Modulus of 1.5 GPa and a Poisson's ratio of 0.3 were assigned to the model. This two dimensional approach was endorsed by Skordos *et al.*[15].

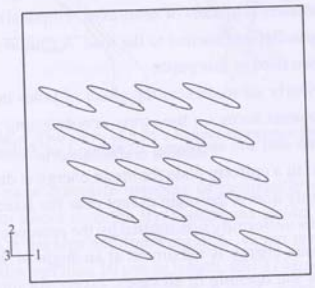

Fig. 6 Multiple hole arrangement derived from the morphology shown in Fig. 3.

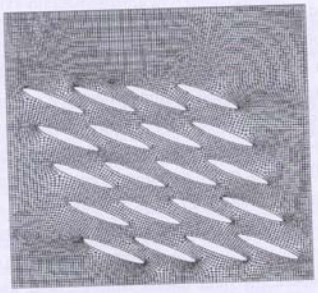

Fig. 7 Mesh for multiple hole model (12 823 elements).

A tensile deformation corresponding to 1% of the model height was applied to the top surface of the mesh. Symmetry boundary conditions were applied to the left hand edge and also the base of the model (i.e. $ux = 0$ at $x = 0$, and $uy = 0$ at $y = 0$). These boundary conditions were chosen as they produce a uniform strain field of 0.01 (1% strain) in a model without holes. Thus, the strain amplification in the model with holes could be quantified readily.

The FE output data concerning nodal coordinates on the extreme periphery of the hole before and after loading were downloaded from the ABAQUS environment into a Microsoft EXCEL spreadsheet. This enabled the calculation of the original distance between the nodal points marking the end of the minor and major axes respectively. The coordinates of the same nodes after loading were also identified and the distances spanned by deformed major and minor axes were similarly calculated. Major and minor axes strains were calculated by dividing each change in axis length by the corresponding original length. These strains are influenced by the mesh density assigned to the problem, with the consequence for this mesh that the strain values calculated have their accuracy limited to +/−0.5%.

2.2 Finite element predictions

The maximum stress in the single-hole model was 60 MPa compared with the maximum value from a model with no holes of 15 MPa, so the stress concentration factor was 60/15 = 4. The distribution of shear strain energy in the loaded plate with the multiple hole arrangement shows that the material around the holes on the top left and bottom right experiences the highest stress concentrations, probably due to the influence of the edges of the plate (Figs. 8, 10). The maximum von Mises stress has also increased in the multiple hole model by a factor of 1.664/1.27 = 1.31 over the single hole model due to the influence of the aspect ratio of the hole. The maximum value here was 166 MPa compared with the maximum value from model with no holes of 15 MPa, so the stress concentration factor was 166/15 = 11.1. A

comparison of the deformed and undeformed model outlines is shown in Fig. 9.

Changes in the major and minor diameters of each of the holes were used to calculate percentage diameter strains of the holes (Tables 1 and 2). The major axis was not sensitive to the applied deformation, but the minor axis showed significant strain amplification. In the single hole model a strain magnification of 9.82 was calculated, consistent with the findings of Skordos *et al.*[15]. In the multiple hole model the largest multiple of the 1% applied strain, i.e. 8.75, was recorded for the bottom right hand hole in the model. It must be noted that at these high strain levels the validity of the linear elastic materials properties used in this model must be called into question. However, for lower applied levels of deformation, these strain amplifications would be valid up to the point of yield.

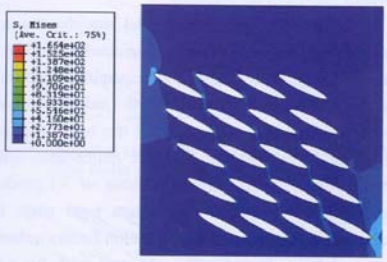

Fig. 8 Distribution of von Mises stress in the loaded plate with multiple holes.

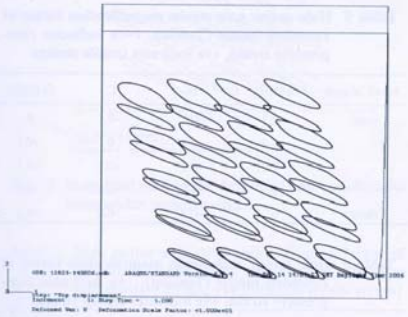

Fig. 9 Comparison of the deformed and undeformed model outlines (displacements magnified by 10).

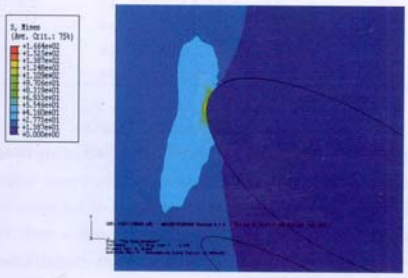

Fig. 10 Enlarged top left corner of Fig. 7.

Table 1 Hole major axis strain magnification factor of initial model (Tension) (−ve indicates compressive strain, +ve indicates tensile strain)

Row/Column	A (left)	B	C	D (right)
1 (top)	−0.4	−0.2	0.2	0
2	−0.3	0.5	−0.2	−0.1
3	−0.2	−0.2	−0.2	−0.2
4	−0.2	−0.1	−0.3	−0.3
5 (base)	−0.2	−0.3	−0.3	−0.5

Table 2 Hole minor axis strain magnification factor of initial model (Tension) (−ve indicates compressive strain, +ve indicates tensile strain)

Row/Column	A (left)	B	C	D (right)
1 (top)	0.8	6.6	6.1	1.4
2	0	2.3	2.4	2.5
3	6.0	6.2	5.4	6.0
4	1.3	3.5	7.0	7.1
5 (base)	0.7	5.6	7.3	8.8

Table 3 Strain energy density predictions from this study compared with Skordos *et al.*

Opening type	Maximum strain energy density (MPa)	Amplification factor
No opening	20.4	
Circular-drilled	221.5	10.9
Circular-formed	93.9	4.60
Normal elliptical-drilled	453.7	22.2
Normal elliptical-formed	197.8	9.70
Parallel elliptical-drilled	94.6	4.64
Parallel elliptical-formed	52.1	2.55
This study: Multiple hole model (off axis elliptical-drilled)	166	11.1

Table 4 Strain amplification predictions from this study compared with Skordos *et al.*

Opening type	Bulk deformation	Parallel to the loading	Normal to the loading
No opening	2.85	2.87 (1.01)	−0.87 (−0.31)
Circular-drilled	2.91	11.90 (4.09)	−5.90 (−2.03)
Circular-formed	2.94	10.80 (3.67)	−9.44 (−3.21)
Elliptical-drilled (major axis normal to load)	2.90	19.30 (6.66)	−4.71 (1.62)
Elliptical-formed (major axis normal to load)	2.92	15.81 (5.47)	−7.01 (−2.40)
Elliptical-drilled (major axis parallel to load)	2.87	7.43 (2.59)	−6.08 (2.12)
Elliptical-formed (major axis parallel to load)	2.92	7.49 (2.57)	−12.77 (−4.37)
Multiple hole model (off axis elliptical-drilled)	1.00	8.75 (8.75+/−0.50)	0.0 (0.0)

In more detail, the stress concentration of Fig. 8 at the top left (and bottom right) corner (Fig. 10) does not affect the overall change in compliance due to the introduction of the holes and so could be ameliorated by the introduction of strengthening at the corners. It is possible that the stiff ring around the campaniform sensilla used in Skordos' model serves a similar protective function.

2.3 Effect of boundary and loading conditions

The behaviour of an extended finite element model was explored in order to establish the influence of boundary and loading conditions. The model used contained the same set of hole geometries, but surrounded by extended supporting material (Fig. 11). Again, changes in the major and minor diameters of each of the holes under tensile loading were used to calculate percentage diameter strains of the holes (Tables 5 and 6). Comparison with Tables 1 and 2 shows that the extended surrounding material acted to generally reduce the overall magnitudes of strain magnification (peak now 6.8 down from 8.8), but with little influence on the overall pattern of deformation.

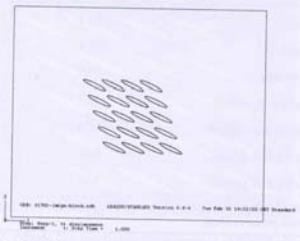

Fig. 11 Geometry of the extended block model.

The extended geometry model was also run under positive and negative shear loading conditions (Figs. 12 and 13). The corresponding hole strain magnification factors are shown in Tables 7 to 10. Under the action of positive shear the minor axis of the holes was more sensitive to the loading than the major axis, with a maximum strain magnification factor of 3.1 predicted for the hole located at the bottom right edge. Less variation in the range of magnification factors across the array of holes is apparent, compared with the corresponding model under tensile loading (Table 6).

Table 5 Hole major axis strain magnification factor of extended model (Tension) (−ve indicates compressive strain, +ve indicates tensile strain)

Row/Column	A (left)	B	C	D (right)
1 (top)	−0.3	−0.1	−0.1	0
2	−0.2	−0.1	0	−0.1
3	−0.2	−0.1	−0.1	−0.1
4	0	−0.1	−0.2	−0.2
5 (base)	0	−0.2	−0.2	−0.3

Table 6 Hole minor axis strain magnification factor of extended model (Tension) (−ve indicates compressive strain, +ve indicates tensile strain)

Row/Column	A (left)	B	C	D (right)
1 (top)	6.5	5.1	3.7	2.3
2	4.0	4.3	3.7	2.8
3	3.4	3.7	4.0	3.4
4	2.6	3.4	4.0	4.3
5 (base)	2.3	3.7	5.1	6.8

The application of negative shear (Fig. 12) was to make the holes longer and thinner, thus producing tensile major axis strains and compressive minor axis strains. For this type of loading, the major axis of the holes was more sensitive to the loading than the minor axis. The variation in the predicted major strain magnification factors is within the measurement error, suggesting an even distribution of strain amplification across the array.

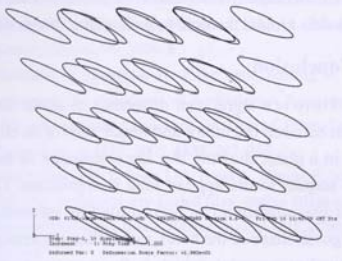

Fig. 12 Magnified view of the deformed and undeformed holes under positive shear.

Fig. 13 Magnified view of the deformed and undeformed holes under negative shear.

Table 7 Hole major axis strain magnification factor of extended model (+ve shear) (−ve indicates compressive strain, +ve indicates tensile strain)

Row/Column	A (left)	B	C	D (right)
1 (top)	−0.2	−0.2	−0.2	−0.2
2	−0.2	−0.2	−0.2	−0.2
3	−0.2	−0.2	−0.1	−0.2
4	−0.2	−0.2	−0.2	−0.2
5 (base)	−0.2	−0.2	−0.2	−0.3

Table 8 Hole minor axis strain magnification factor of extended model (+ve shear) (−ve indicates compressive strain, +ve indicates tensile strain)

Row/Colum	A (left)	B	C	D (right)
1 (top)	2.8	2.8	2.0	1.4
2	2.3	1.7	1.7	1.7
3	2.3	1.7	1.7	2.0
4	1.7	1.7	2.0	2.3
5 (base)	1.7	2.0	2.3	3.1

Table 9 Hole major axis strain magnification factor of extended model (−ve shear) (−ve indicates compressive strain, +ve indicates tensile strain)

Row/Colum	A (left)	B	C	D (right)
1 (top)	4.1	4.1	4.0	4.0
2	4.0	3.9	3.9	4.0
3	4.0	4.0	3.9	4.0
4	3.9	3.9	4.0	4.0
5 (base)	3.9	4.0	4.0	4.1

Table 10 Hole minor axis strain magnification factor of extended model (−ve shear) (−ve indicates compressive strain, +ve indicates tensile strain)

Row/Colum	A(left)	B	C	D(right)
1 (top)	−2.7	−2.4	−1.7	−1.4
2	−2.0	−1.7	−1.7	−1.7
3	−2.0	−1.7	−1.7	−2.0
4	−1.7	−1.7	−2.0	−2.0
5 (base)	−1.4	−1.7	−2.0	−2.7

Comparison across Tables 5 to 10 indicates the tensile loading produced the maximum strain magnification which was highly localised. Shear loading produced lower peak magnifications, but a more even distribution across the holes in the array.

3 Further work

Further work must address the following topics:

(1) The effect of the *aspect ratio* of the hole (reaching its extreme form in the slit sensillum) in terms both of its sensitivity and (as a corollary) its effect on the compliance of the plate in which it is embedded.

(2) The effect of *orientation* of the hole on sensitivity to deformations in particular directions.

(3) The directional effect of *imposed strains with respect to anisotropy* due to the orientation of embedded fibres in the plate.

(4) The *influence of other holes* in the vicinity. Since the inclusion of a hole has as its primary effect the local increase in compliance, and since in an array of holes (perhaps 100 holes arranged in a 10×10 array) placed sufficiently close together there will therefore be a gradient in compliance across the array, it is immediately apparent that the system will have a range of characteristic response times across the array, and so be tuned to a range of input frequencies.

(5) The *material* from which the plate and sensillum are made. This includes the variables normally associated with composite materials, but also others such as silicon, metals, *etc*.

(6) The design of *ancillary components* of the hole (in arthropods the cap is regarded as an ancillary item) that can make the deformation of the hole easier to detect by standard displacement detectors, integral or remote[28]. This is a function both of the basic geometry of the system, and of the materials used to connect the ancillary components to the hole.

(7) In a blind-hole MEMS system the conformation of the membrane (flat or domed) affects the degree of strain amplification.

There are many options for the detection of the change in shape of the hole (see also Table 1 from Skordos *et al.* 2002). In nature the displacement of the cap stimulates a cell, and this displacement could be detected by a strain gauge or by a ranging laser. Other options are:

(1) Fill the hole with a soft polymer that changes shape as the hole is deformed (e.g. form a dome). If the polymer were plastic this could be incorporated into a tell-tale to be monitored after the mission.

(2) Add conducting particles to the soft polymer so that the capacitance or resistance of the polymer will be changed.

(3) Fill the hole with a birefringent material that will respond by changing its response to polarised radiation as the hole is deformed.

(4) Line the sides of the hole with a reflective material so that the path length of a ray entering the hole at grazing incidence can be reflected several times by the sides of the hole before it exits.

(5) During fabrication arrange for a thin web of piezoelectric material to be left closing the hole and measure strains in this web[29].

(6) Leave a thin web of material across the hole, perhaps domed, detecting strains in this web using laser-based remote sensing[30].

(7) Detect changes in the deformation of the material surrounding the hole: strain can be concentrated in relatively "safe" areas by manipulating the orientation of fibres around the hole[15].

(8) Arrange fibres (optical or piezoelectric) within the matrix around the hole to pick up the strains directly.

4 Conclusion

There is a significant difference in strain magnification between the minor and major axes of an elliptical hole in a plate, showing that the orientation of the hole with respect to the applied load is significant. Greater strain magnification can be recorded by measuring the changes in shape of the holes, rather than the strain in the surrounding material, which is the parameter an engineer would tend to measure. Thus it is possible to produce useful strain magnification without compromising the integrity of the surrounding material. From an engineering point of view this is counterintuitive. In a group of holes the dangerous stress concentrations are fewer than might be expected and can be guarded against without compromising the central concept presented here – the local control of compliance to amplify global strain.

The effects of grouping and mutual proximity of the holes remain to be explored in detail; biological systems use the size of the sensor as a primary filter to fractionate the signal. This peripheral conditioning will reduce the amount of information transmitted and increase the efficiency of the system.

Acknowledgements

This research was carried out during a joint collaboration between University of Bath and the Advanced Concepts Team of ESA in the framework of the Ariadna program.

References

[1] Cao L, Kim T S, Mantell S C, Polla D L. Simulations and fabrication of piezoresistive membrane type MEMS strain sensors. *Sensors and Actuators, A: Physical*, 2000, **80**, 273–279.

[2] Menadier C, Kissinger C, Adkins H. The fotonic sensor. *Instruments and Control Systems*, 1967, **40**, 114–120.

[3] Wnuk S P Jr, Wnuk V P. The Development of a PdCr Integral Weldable Strain Measurement System Based on NASA Lewis PdCr/Pt Strain Sensor for User-Friendly Elevated Temperature Strain Measurements. NASA Contractor Report 202316, 1997.

[4] Ounaies Z, Harrison J S, Silcox R J. Piezoelectric materials for sensor and actuator applications at NASA LaRC. *ICASE Research Quarterly*, 1999, **8**.

[5] Mckenzie L, Karafolas N. Fiber optic sensing in space structures: The experience of the European Space Agency. *17th International Conference on Optical Fibre Sensors, Proceedings of SPIE*, 2005, **5855**, 262–269.

[6] Udd E, Schulz W L, Seim J M, Trego A, Haugse E, Johnson P E. Use of transversely loaded fiber grating strain sensors for aerospace applications. *Proceedings of SPIE*, 2000, **3994**, 96–104.

[7] Dubois P, Menon C, Shea H. Ad-hoc wireless sensor networks for exploration of solar-system bodies. *57th International Astronautical Congress*, Valencia, Spain, 2006.

[8] Peng S, O'Keeffe J, Wei C Y, Cho K, Kong J, Chen R, Franklin N, Dai H. Carbon nanotube chemical and mechanical sensors. *The 3rd International Workshop on Structural Health Monitoring*, Stanford University, USA, 2001.

[9] Andersen S O. Exoskeletal proteins from the crab. *Cancer pagurus. Comparative Biochemistry and Physiology A: Molecular and Integrative Physiology*, 1999, **123**, 203–211.

[10] Delcomyn F, Nelson M E, Cocatre-Zilgien J H. Sense organs of insect legs and the selection of sensors for agile walking robots. *The International Journal of Robotics Research*, 1996, **15**, 113–127.

[11] Bashir R, Gupta A, Neudeck G W, McElfresh M, Gomez R. On the design of piezoresistive silicon cantilevers with stress concentration regions for scanning probe microscopy applications. *Journal of Micromechanics and Microengineering*, 2000, **10**, 483–491.

[12] Wicaksono D H B, Zhang L J, Pandraud G, French P J, Vincent J F V. Fly's proprioception-inspired micromachined strain-sensing structure: Idea, design, modeling and simulation, and comparison with experimental results. *Journal of Physics: Conference Series*, 2006, **34**, 336–341.

[13] Vincent J F V, Wegst U G K. Design and mechanical properties of insect cuticle. *Arthropod Structure and Development*, 2004, **33**, 187–199.

[14] Pringle J W S. Proprioception in insects: II. The action of the campaniform sensilla on the legs. *Journal of Experimental Biology*, 1938, **15**, 114–131.

[15] Skordos A, Chan P H, Vincent J F V, Jeronimidis G. A novel strain sensor based on the campaniform sensillum of insects. *Philosophical Transactions of the Royal Society A: Mathematical, Physical and Engineering Sciences*, 2002, **360**, 239–254.

[16] Zill S N, Moran D T. The exoskeleton and insect proprioception. I. Responses of tibial campaniform sensilla to external and muscle-generated forces in the American cockroach, Periplaneta americana. *Journal of Experimental Biology*, 1981, **91**, 1–24.

[17] Zill S N, Moran D T. The exoskeleton and insect proprioception: III. Activity of tibial campaniform sensilla during walking in the American cockroach, Periplaneta americana. *Journal of Experimental Biology*, 1981, **94**, 57–75.

[18] Dickinson M H. Linear and nonlinear encoding properties of an identified mechanoreceptor on the fly wing measured with mechanical noise stimuli. *Journal of Experimental Biology*, 1990, **151**, 219–244.

[19] Keil T A. Functional morphology of insect mechanoreceptors. *Microscopy Research and Technique*, 1997, **39**, 506–531.

[20] Keil T A. Comparative morphogenesis of sensilla: A review. *International Journal of Insect Morphology and Embryology*, 1997, **26**, 151–160.

[21] Gruenert U, Gnatzy W. Campaniform sensilla of *Calliphora vicina* (Insecta, Diptera) II. Typology. *Zoomorphology*, 1987, **106**, 320–328.

[22] Chapman K M, Mosinger J L, Duckrow R B. The role of distributed viscoelastic coupling in sensory adaptation in an insect mechanoreceptor. *Journal of Comparative Physiology A: Neuroethology, Sensory, Neural and Behavioral Physiology*, 1979, **131**, 1–12.

[23] Gnatzy W, Gruenert U, Bender M. Campaniform sensilla of *Calliphora vicina* (Insecta, Diptera) I. Topography. *Zoomorphology*, 1987, **106**, 312–319.

[24] Pringle J W S. The gyroscopic mechanism of the halteres of Diptera. *Philosophical Transactions of the Royal Society B: Biological Sciences*, 1948, **233**, 347–384.

[25] Harvey J. *Global Energy Absorption through Local Compliance Control*, 2005.

[26] Chen B, Peng X, Wang W, Zhang J, Zhang R. Research on the microstructure of insect cuticle and the strength of a biomimetic preformed hole composite. *Micron*, 2002, **33**, 571–574.

[27] Wigglesworth V B. *The Principles of Insect Physiology*, 7th ed, Chapman and Hall, London, 1972.

[28] Motamed M, Yan J. A review of biological, biomimetic and miniature force sensing for microflight. *IEEE/RSJ International Conference on Intelligent Robots and Systems (IROS)*, Edmonton, Alberta, Canada, 2005, 3939–3946.

[29] Niezrecki C, Brei D, Balakrishnan S, Moskalik A. Piezoelectric actuation: State of the art. *The Shock and Vibration Digest*, 2001, **33**, 269–280.

[30] Wicaksono D H B, Vincent J F V, Pandraud G, Craciun G, French P J. Biomimetic strain-sensing microstructure for improved strain sensor: Fabrication results and optical characterization. *Journal of Micromechanics and Microengineering*, 2005, **15**, S72–S81.

Erratum

The Editorial Office apologizes for a mistake that occurred in Vol. 3, No. 3, pages 127–138. In the article "Computational Models to Synthesize Human Walking" the **Acknowledgement** part was wrongly published, which should be deleted.